Branching Fractions for H_2O Forming Channels of the Reaction of OH Radicals with Acetaldehyde

N. I. Butkovskaya,* A. Kukui,† and G. Le Bras

CNRS, Laboratoire de Combustion et Systèmes Réactifs, 1C Av. de la Recherche Scientifique, 45071 Orléans Cedex 2, France and CNRS, Service d'Aéronomie, Paris, France

Received: September 15, 2003; In Final Form: November 29, 2003

Branching fractions for two hydrogen abstraction channels of the OH + CH_3CHO reaction producing H_2O + CH_3CO (a) and H_2O + CH_2CHO (b) were determined using chemical ionization mass spectrometry. Reaction took place in a high-pressure turbulent flow reactor at 200 Torr of carrier gas N_2. The branching fraction for the abstraction from the methyl group, $(5.1^{+2.4}/_{-1.7})$ %, was determined at room temperature by direct detection of the vinoxy radicals (CH_2CHO) using proton-transfer ionization. The total H_2O yield of (97.7 ± 4.7) % was obtained at $T = 298$ and 248 K by comparison with OH + C_6H_{12} reaction, confirming that in this temperature range reaction proceeds by H-atom abstraction. Secondary reactions of the acetyl and vinoxy radicals in the presence of O_2 and NO_2 were studied by monitoring the stable products CH_2O, $(HCO)_2$, and CH_3OH using proton-transfer ionization. It was found that formaldehyde is the major coproduct of OH in the CH_3CO + O_2 reaction.

Introduction

Oxidation of acetaldehyde in the troposphere is an efficient source of peroxyacetylnitrate (PAN), which is a reservoir for NO_x (NO, NO_2) species, the latter playing an important role in the photochemical ozone production. PAN is also a hazardous pollutant. Acetaldehyde is emitted into the atmosphere from anthropogenic and biogenic sources or can be produced in photooxidation of other organic compounds. Degradation of acetaldehyde in the atmosphere is initiated mainly by reaction with hydroxyl radicals, for which a negative temperature dependence of the reaction rate constant in 201−550 K range was established with $k_1 = (1.5 \pm 0.2) \times 10^{-11}$ cm^3 molecule^{-1} s^{-1} at 298 K.[1,2] The negative temperature dependence has led to suggest that this reaction proceeds, at least partly, via the formation of an intermediate complex. The reaction mechanism has been studied at different temperatures,[3−6] and four possible channels have been considered:

$$\mathrm{OH + CH_3CHO \rightarrow CH_3CO + H_2O} \quad (1a)$$

$$\rightarrow \mathrm{CH_2CHO + H_2O} \quad (1b)$$

$$\rightarrow \mathrm{(CH_3CHO{\cdot}OH) \rightarrow CH_3 + HCOOH} \quad (1c)$$

$$\rightarrow \mathrm{(CH_3CHO{\cdot}OH) \rightarrow H + CH_3COOH} \quad (1d)$$

Channels 1a and 1b proceed by abstraction of H-atom, respectively, from the carbonyl and methyl groups. Since the C−H bond dissociation energies in the methyl group is substantially higher than in the carbonyl group (D_0(H−CH_2-CHO) = 92.8 kcal mol^{-1} and D_0(CH_3C(O)−H) = 87.9 kcal mol^{-1}),[7] channel 1a is expected to be the preferential pathway. This is confirmed by the yield of acetyl radicals, CH_3CO, of 0.93 ± 0.18 at 296 K found by Cameron et al.[5] The two other pathways, 1c and 1d, were suggested by Taylor et al.[3] on the basis of the negative temperature dependence of k_1, which was attributed to the formation of an adduct followed by decomposition forming CH_3 or H radicals. However, the upper limits for the formation yields of CH_3 (0.03) and H (0.02) determined by Cameron et al.[5] do not support the occurrence of these channels in the 237−298 K range of their study. Additional evidence against the significance of the addition−elimination reaction pathways 1c and 1d was found both by Vandenberk and Peeters,[6] who set an upper limit of 3% to the yield of formic acid and determined a yield of 89 ± 16% for H_2O, and by Tyndall et al.,[4] who measured a yield less than 10% for the sum formation of formic and acetic acids. These experimental findings were confirmed by theoretical studies where high level ab initio calculations provided a large barrier height to the formation of the ($CH_3CHO{\cdot}OH$) complex.[8,9] These recent detailed studies of the reaction products,[4−6] however, did not include a quantitative investigation of channel 1b. Its rate coefficient was estimated using transition-state theory,[3,9] but this reaction has never been observed experimentally.

In the present work, the branching ratios of the hydrogen abstraction channels were determined using the advantages of chemical ionization mass spectrometry (CIMS) technique. The vinoxy radical, CH_2CHO, was directly detected by proton transfer. To calibrate the CH_2CHO mass spectrometric signal, the reaction of acetaldehyde with F atoms with a known branching ratio was used:[10]

$$\mathrm{F + CH_3CHO \rightarrow HF + CH_3CO} \quad (2a)$$

$$\rightarrow \mathrm{HF + CH_2CHO} \quad (2b)$$

Kinetics of the primary radicals from reactions 1 and 2 were examined to find the conditions when their concentrations are not noticeably affected by the secondary reactions and comparison of the CH_2CHO signals from reactions 1 and 2 permits to determine the branching fraction of channel 1b. The total

* Permanent address: Institute of Chemical Physics of the Russian Academy of Sciences, 117334 Moscow, Russian Federation.

† Service d'Aéronomie.

10.1021/jp036740m CCC: $27.50
Published on Web 01/20/2004

H_2O yield from channels 1a + 1b was estimated by comparison of the H_2O peak intensity with that from the OH reaction with cyclohexane which has a unity H_2O yield.[11]

Stable products CH_2O, $(HCO)_2$, and CH_3OH were also detected in OH + CH_3CHO and F + CH_3CHO systems using proton-transfer ionization. Kinetics of these products were studied in the presence of O_2 and NO_2 at different concentrations to elucidate the oxidation mechanisms of the primary CH_3CO and CH_2CHO radicals.

Experimental Section

Chemical Reactor. The title reaction was studied in a high-pressure turbulent flow reactor (HPTFR) coupled with chemical ionization mass spectrometer (CIMS). The reactor was a Pyrex tube of 2.4 cm inner diameter. The pressure in the reactor was 200 Torr; the flow velocity of N_2 carrier gas was 18 m/s. Mixing and flow conditions were determined by the Reynolds number (Re = 7300), which ensured a plug flow and a turbulent mixing of reagents. A detailed description of the experimental setup and validation of the flow conditions was presented in the previous work from this laboratory.[12] In particular, the effective flow velocity in the reactor is equal to $(1.23 \pm 0.12)\cdot v$, where v is the velocity calculated from the volumetric flow rate. A total flow of about 96 STPL min^{-1} was obtained with N_2 drawn from a liquid nitrogen tank. Before entering the reactor, N_2 passed successively through a stainless steel cylinder containing BASF Cu catalyst R3−11G removing O_2 and a glass reservoir with molecular sieves trapping H_2O. Without the Cu-catalyst filter, the O_2 concentration in the reactor was about 10^{14} molecule cm^{-3}. The filter allowed lowering this concentration by 1 order of magnitude as determined mass spectrometrically by flowing a known concentration of O_2 into the reactor.

A movable injector of 1.1 cm inner diameter served as a prereactor to produce OH radicals in reaction:

$$H + NO_2 \rightarrow OH + NO \qquad (3)$$

H-atoms were generated by the microwave discharge of H_2/He gas mixtures in a quartz tube of 0.6 cm inner diameter concentrically connected with the injector. To produce reaction 2, F_2/He mixture was used without introduction of NO_2. Tank grade H_2 and F_2 (Alpha Gas 2) were used without further purification. NO_2 was purified by keeping its mixture with O_2 during 24 h followed by pumping out the oxygen through the liquid N_2 trap. After that, NO_2 diluted in He (∼10%) was stored in a glass flask. Concentration of NO_2 in the injector was about 1×10^{13} molecule cm^{-3}, which was sufficient to consume totally the H-atoms within the 2 ms residence time in the injector. The average flow velocity of nitrogen in the injector was about 40 m/s. The maximal distance from the injector tip to the orifice of the inlet cone of the mass spectrometer was 55 cm, which corresponded to a reaction time in the HPTFR of 35 ms. The previous flow tests[12] showed that at Re > 2300 the minimal distance at which the turbulent mixing provided an accurate measurement of the reaction rates was 3 cm. In the present study, this distance corresponded to a reaction time of 1.7 ms. Kinetic measurements in several chemical systems showed that appearance of the primary and secondary products at reaction time as short as 2 ms was in good agreement with the calculated time profiles. For example, in formation of $CH_3S(O)OH$ and SO_2 in OH + $(CH_3)SO$ system,[12] deviation from the expected values was within the experimental error limits. The OH radical signal was calibrated by measuring the consumption of excess NO_2 in reaction 3 by introducing NO_2 into the main reactor. The F atoms concentration was determined by chemical titration using the fast F + CH_3CHO reaction.

Acetaldehyde (Fluka, 99,9%) was introduced into the reactor upstream of the tip of the movable injector. Its flow rate was measured using a manometrically prepared mixture in He and its concentration was varied in the range of $(3 \div 70) \times 10^{12}$ molecule cm^{-3}. The CIMS signals representing acetaldehyde and NO_2 were linear in the $(1 \div 70) \times 10^{12}$ and $(0.8 \div 20) \times 10^{12}$ molecule cm^{-3} ranges, respectively.

Ion-Molecular Reactor. The ion-molecular reactor (IMR) was a stainless steel tube of 4 cm diameter and 40 cm length located perpendicular to both the chemical reactor and the rods of the quadrupole analyzer (EXTREL). The Ar carrier gas was purified by passing through a liquid N_2 trap. The flow velocity of Ar was 20 m s^{-1} at 0.7 Torr pressure. The primary Ar^+ ions and free electrons were generated in the ion source with a heated filament. SF_6 was continuously introduced into the IMR downstream of the ion source. The primary SF_6^- negative ions were produced by attachment of thermalized electrons to SF_6. Hydroxyl radicals and NO_2 were detected as OH^- (*m*/*e* 17) and NO_2^- (*m*/*e* 46) ions formed by electron transfer from SF_6^-.[12] Water molecules produced in reaction 1 were detected as H_2O^+ ions (*m*/*e* 18) using He flow purified by passing successively through two traps cooled by liquid N_2. Water molecules entering the ion source from the chemical reactor were ionized by charge-transfer reactions with He^+.

Acetaldehyde and primary CH_2CHO radicals were detected using proton transfer from H_3O^+ ion. To produce H_3O^+ ions, H_2O was flowed into the IMR downstream of the ion source along with SF_6. The H_2O flow was created by directing a fraction of the Ar flow over the surface of distilled water in the trap attached to the IMR via a regulating valve. The orifice of the sampling cone of the main reactor was located 8.5 cm downstream of the H_2O flow entrance, so that the following reactions took place prior to reaction between the ions and the neutral species from the chemical reactor:[13]

$$Ar^+ + H_2O \rightarrow H_2O^+ + Ar$$
$$\rightarrow ArH^+ + OH$$
$$H_2O^+ + H_2O \rightarrow H_3O^+ + OH$$
$$Ar^+H + H_2O \rightarrow H_3O^+ + Ar$$

The H_2O flow was regulated in such a manner that all Ar^+ and H_2O^+ ions reacted with H_2O, and in the absence of reactants in the chemical reactor the major observed positive ions in the IMR were H_3O^+ and its water clusters $H_3O^+\cdot(H_2O)_{n+1}$ with $n = 0-2$ formed in the sequential reactions:

$$H_2O^+\cdot(H_2O)_n + H_2O \leftrightarrow H_3O^+\cdot(H_2O)_{n+1}$$

Acetaldehyde was detected using the proton-transfer reaction:

$$H_3O^+ + CH_3CHO \rightarrow C_2H_5O^+ + H_2O$$

giving a peak at *m*/*e* 45, while the clusters react presumably via ligand switching.[14] In these conditions, practically no signal from acetaldehyde was observed at *m*/*e* 44 corresponding to the parent CH_3CHO ion. The mass spectrum of positive ions with 7×10^{12} molecule cm^{-3} of acetaldehyde in the main reactor is presented in Figure 1a.

Direct detection of CH_2CHO radicals by CIMS was possible owing to the different proton affinities (PA) of CH_3CO and

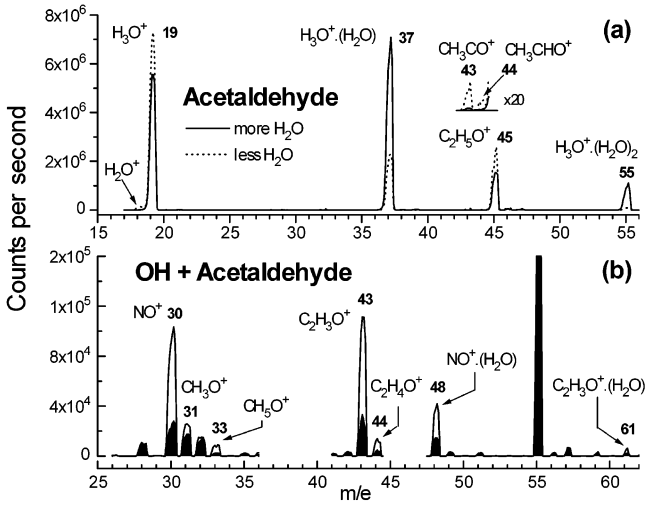

Figure 1. Registration of acetaldehyde and products of its reaction with OH using proton-transfer reaction with H_3O^+. Top panel: mass spectra in the presence of more (solid lines) and less (dotted lines) amounts of water in the IMR with $[CH_3CHO] = 7 \times 10^{12}$ molecule cm^{-3} in HPTFR. Bottom panel: mass spectra with discharge on (white areas) and discharge off (black areas) at $t = 8$ ms with $[CH_3CHO] = 9 \times 10^{12}$, $[NO_2] = 8 \times 10^{12}$, and $[OH] \approx 1 \times 10^{12}$ molecule cm^{-3}. See text for the detailed assignment of the observed peaks.

CH_2CHO radicals, 156 and 185 kcal/mol, respectively.[15] Since the PA of H_2O, 165 kcal/mol, falls between these two values, proton transfer from H_3O^+ to acetyl radical does not occur and only the ion-molecular reaction

$$H_3O^+ + CH_2CHO \rightarrow C_2H_4O^+ + H_2O \qquad (4)$$

or its cluster analogue with $H_3O^+\cdot(H_2O)_n$ can give a signal at *m*/*e* 44. Figure 1b illustrates the change of line intensities after switching on the discharge generating OH radicals. We see that both *m*/*e* 44 and *m*/*e* 43 peaks increase in the presence of reaction. The increase of the signal at *m*/*e* 44 is entirely due to CH_2CHO radicals, while the peak at *m*/*e* 43 needs more detailed consideration.

The peak at *m*/*e* 43, CH_3CO^+ ion, can originate either directly from acetyl radical or as a fragment from other products containing acetyl group. Acetyl radical has a very low ionization potential, 7 eV, and the acetyl ion could be produced in the reaction:

$$H_3O^+ + CH_3CO \rightarrow CH_3CO^+ + H_2O + H \qquad (5)$$

which is exothermic by 8 kcal mol^{-1} (the analogous reaction with NO is known to occur and to give a NO^+ signal at *m*/*e* 30[13]). On the other hand, in the presence of oxygen, acetyl radicals are rapidly converted into peroxyacetyl radicals[1], $CH_3C(O)OO$, and at $[O_2] \approx 10^{14}$ molecule cm^{-3}, which corresponds to the background O_2 concentration in the reactor, the conversion is complete within a few milliseconds, whereas the signal at *m*/*e* 43 was observed in a full range of residence time in the main reactor even when the N_2 flow was not purified from oxygen. This indicates that $CH_3C(O)OO$ radicals can contribute to *m*/*e* 43. The following reaction:

$$H_3O^+ + CH_3C(O)OO \rightarrow CH_3CO^+ + H_2O + HO_2 \qquad (6)$$

is energetically possible and can be responsible for the signal at *m*/*e* 43, but contribution from other products is not excluded. We did not find any response at *m*/*e* 75 ($C_2H_3O_3^+$) or 76 ($C_2H_4O_3^+$) in the positive mode, but in the negative spectra from the title reaction, a signal at *m*/*e* 75 was found which could be attributed to $CH_3C(O)OO$ radicals (vide infra). Using $H_3O^+(H_2O)_n$ ions, organic products with PA greater than that of water, such as CH_2O (170.4 kcal mol^{-1}), CH_2CO (197.3 kcal mol^{-1}), and CH_3OH (180.3 kcal mol^{-1}),[15] can be detected by proton transfer:[13,14]

$$H_3O^+ + CH_2O \rightarrow CH_3O^+ + H_2O$$

$$H_3O^+ + CH_2CO \rightarrow C_2H_3O^+ + H_2O$$

$$H_3O^+ + CH_3OH \rightarrow CH_5O^+ + H_2O$$

Among them, ketene, CH_2CO, can also contribute to the signal at *m*/*e* 43. Formaldehyde and methanol give signals at *m*/*e* 31 and 33, respectively. Detection of these molecules made it possible to reveal some details of the mechanism of CH_3CO and CH_2CHO oxidation. A detailed assignment of the observed peaks will be discussed below along with consideration of the reaction mechanism.

Results and Discussion

Determination of the Yield of CH_2CHO Radicals. The branching fraction of channel 1b was determined as the ratio of the produced concentration of the vinoxy radicals to the consumed concentration of OH radicals in reaction 1:

$$\Phi(CH_2CHO) = \Delta[CH_2CHO]/\Delta[OH] \qquad (E1)$$

The measured intensity of the vinoxy radicals from reaction 1 was quantified using reaction 2:

$$F + CH_3CHO \rightarrow HF + CH_3CO \qquad (2a)$$

$$\rightarrow HF + CH_2CHO \qquad (2b)$$

with the known branching ratio, $k_{2a}/k_{2b} = (65 \pm 9\%)/(35 \pm 9\%) = 1.86(+1.0/-0.6)$ at 298 K:[10]

$$\Delta[CH_2CHO] = (I_{44})_{OH}\cdot\Delta[F]\cdot 0.35/(I_{44})_F \qquad (E2)$$

where $(I_{44})_{OH}$ and $(I_{44})_F$ are the CH_2CHO intensities measured from reactions 1 and 2, respectively, and $\Delta[F]$ is the consumed concentration of F atoms. As reaction 2 is very fast, $k_7 = 1.4 \times 10^{-10}$ cm^3 $molecule^{-1}$ s^{-1},[10] $\Delta[F]$ is equal to the initial concentration of F atoms. The obtained branching ratio is correct if at the moment of measurement the change of CH_2CHO radicals concentration because of secondary reactions is negligible. To validate the conditions for the measurements of the primary yield of vinoxy radicals and to confirm the assignment of the observed peaks, the kinetics of the CH_2CHO, CH_3CO, $CH_3C(O)O_2$, and OH radicals produced in reactions 1 and 2 were investigated at different oxygen concentrations.

Time profiles of these products are presented in Figure 2. Upper row shows signal intensities of positive ions at *m*/*e* 43 and 44, and lower row shows negative ion intensities at *m*/*e* 17 and 75. Vertical pairs of plots represent the following reactions: (a) and (a′) $F + CH_3CHO$ with $[O_2] = 3 \times 10^{13}$ molecule cm^{-3} (with oxygen removal catalyst); (b) and (b′) $F + CH_3CHO$ with $[O_2] = 4 \times 10^{14}$ molecule cm^{-3} (without oxygen filter); (c) and (c′) $OH + CH_3CHO$ with $[O_2] = 4 \times 10^{14}$ molecule cm^{-3}. Both reactions 1 and 2 were examined in excess of CH_3CHO to avoid secondary reactions of F atoms and OH radicals. Solid curves correspond to numerical calculations using the reaction scheme given in Table 1. For the sake of simplicity, the known reactions between CH_3, CH_3O_2, CH_3O, and HCO

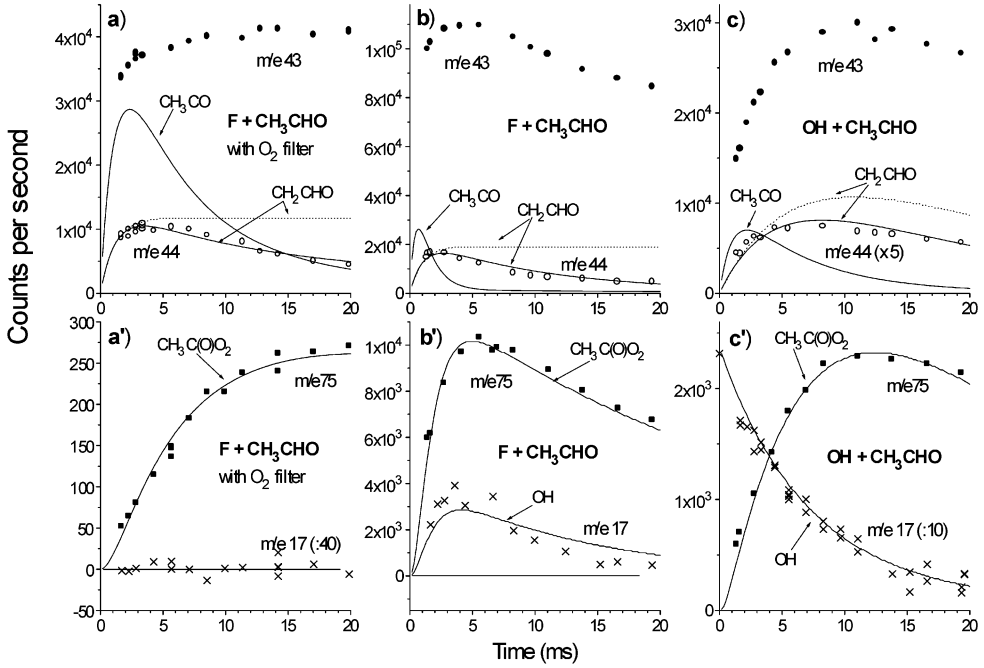

Figure 2. Time profiles of the products of F + CH_3CHO and OH + CH_3CHO reactions measured in positive (top) and negative (bottom) modes. Initial concentration of acetaldehyde was [CH_3CHO] = 7×10^{12} molecule cm^{-3}. Concentrations of other reactants in the reactor: (a) [F] = 1.0×10^{12}, [O_2] = 3×10^{13} with O_2 filter; (b) [F] = 1.1×10^{12}, [O_2] = 4×10^{14}; (c) [OH] = 1.0×10^{12}, [NO_2] = 2.0×10^{12}, and [O_2] = 4×10^{14} molecule cm^{-3}. Solid curves show the results of calculation; dotted curves are from the calculation without account of the secondary reaction of CH_2CHO radical with O_2.

TABLE 1: Simplified Reaction Scheme Used to Model Reactions of OH and F with CH_3CHO in the HPTFR

N	$k(298)^a$	reaction	N	$k(298)^a$	reaction
1a	14.3	$OH + CH_3CHO \rightarrow CH_3CO + H_2O$	15[g]	16	$NO_2 + CH_2CHO \rightarrow CH_2O + HCO + NO$
1b[b]	0.75	$OH + CH_3CHO \rightarrow CH_2CHO + H_2O$	19[i]	8.8	$NO_2 + OOCH_2CHO \rightarrow PVN$
2a	91	$F + CH_3CHO \rightarrow CH_3CO + HF$	20	241	$NO + CH_3CO \rightarrow CH_3CONO$
2b	49	$F + CH_3CHO \rightarrow CH_2CHO + HF$	21	25	$NO + CH_2CHO \rightarrow NOCH_2CHO$
7a	3.4	$O_2 + CH_3CO \rightarrow CH_3C(O)O_2$	22	18	$NO + CH_3C(O)O_2 \rightarrow CH_3 + CO_2 + NO_2$
7b[c]	0.2	$O_2 + CH_3CO \rightarrow ? + OH$	23[i]	8	$NO + OOCH_2CHO \rightarrow CH_2O + HCO + NO_2$
7c[c]	0.5	$O_2 + CH_3CO \rightarrow CH_2O + OH$	24	16	$CH_3C(O)O_2 + CH_3C(O)O_2 \rightarrow 2CH_3 + 2CO_2 + O_2$
8a	0.100	$O_2 + CH_2CHO \rightarrow OOCH_2CHO$	25	1.0	$CH_3 + O_2 \rightarrow CH_3O_2$
8b[d]	0.024	$O_2 + CH_2CHO \rightarrow (HCO)_2 + OH$	26[f]	40	$CH_3O_2 + CH_2CHO \rightarrow CH_2O + CH_3O + HCO$
8c[c]	0.036	$O_2 + CH_2CHO \rightarrow CH_2O + OH + CO$	27	4.5	$CH_3O_2 + CH_3C(O)O_2 \rightarrow CH_3 + CH_3O + CO_2 + O_2$
9a[e]	20	$CH_3CO + CH_2CHO \rightarrow CH_3COCH_2CHO$	28	4.5	$CH_3O_2 + CH_3C(O)O_2 \rightarrow CH_2O + CH_3COOH + O_2$
9b[e]	8	$CH_3CO + CH_2CHO \rightarrow CH_3CHO + CH_2CO$	29	0.2	$CH_3O + CH_3CHO \rightarrow CH_3OH + CH_3CO$
10a[e]	20	$CH_2CHO + CH_2CHO \rightarrow HOC(CH_2)_2CHO$	30[h]	10	$CH_3O + CH_2CHO \rightarrow CH_2CO + CH_3OH$
10b[e]	8	$CH_2CHO + CH_2CHO \rightarrow CH_3CHO + CH_2CO$	31[j]	40	$CH_3 + CH_3C(O)O_2 \rightarrow CH_3 + CH_3O + CO_2$
11[f]	40	$CH_3C(O)O_2 + CH_2CHO \rightarrow CH_3 + CO_2 + CH_2O + HCO$	32	120	$CH_3 + OH \rightarrow CH_3OH$
12a	20	$CH_3CO + CH_3CO \rightarrow (CH_3CO)_2$			
12b	8.4	$CH_3CO + CH_3CO \rightarrow CH_3CHO + CH_2CO$			
13	25	$NO_2 + CH_3CO \rightarrow CH_3 + NO + CO_2$			
14	8.3	$NO_2 + CH_3C(O)O_2 \rightarrow CH_3C(O)O_2NO_2$			

[a] Rate constants (in the units of 10^{-12} cm^3 $molecule^{-1}$ s^{-1}) were taken from the NIST kinetic database[16] except the specified cases. [b] This work. [c] Fitted value. [d] Reference 19. [e] Analogy to 3 and 4. [f] Equal to $k(CH_3O_2 + C_2H_5)$. [g] Lower limit from ref 21. [h] Equal to $k(CH_3O + CH_3CO)$. [i] Equal to $k(NO_2,NO + C_2H_5O_2)$. [j] Equal to $k(CH_3 + CH_3O_2)$.

radicals and their reactions with NO and NO_2, which were taken into account in calculations, were skipped from the presented scheme. Reaction rate constants were taken from the NIST kinetic database[16] or evaluated as specified.

In reaction with F atoms, fast formation of the primary radicals is followed by decay because of their reactions with oxygen:

$$CH_3CO + O_2 + M \rightarrow CH_3C(O)O_2 + \text{other products} \quad (7)$$

$$CH_2CHO + O_2 \rightarrow \text{products}$$

and recombination reactions: (8)

$$CH_3CO + CH_2CHO \rightarrow \text{products} \quad (9)$$

$$CH_2CHO + CH_2CHO \rightarrow \text{products} \quad (10)$$

Reaction 7 with rate constant $k_7 = 4.1 \times 10^{-12}$ cm^3 $molecule^{-1}$ s^{-1} rapidly converts acetyl radicals to peroxy form,[17] so that reaction 11 must be taken into account:

$$CH_3C(O)O_2 + CH_2CHO \rightarrow \text{products} \quad (11)$$

As there are no data for reactions 9−11, reactions 9 and 10 were assumed to proceed analogously to the known CH_3CO self-reaction:

$$CH_3CO + CH_3CO \rightarrow (CH_3CO)_2 \quad (12a)$$

$$\rightarrow CH_3CHO + CH_2CO \quad (12b)$$

with $k_{12a} = 2 \times 10^{-11}$ cm^3 $molecule^{-1}$ s^{-1} (the average from the five recent absolute values[16]) and $k_{12b} = 0.42 \cdot k_{12a} = 8.4 \times$

10^{-12} cm^3 molecule^{-1} s^{-1}.[18] For reaction 11, a value of $k_{11} = 4 \times 10^{-11}$ cm^3 molecule^{-1} s^{-1} was adopted using analogy with $CH_3O_2 + C_2H_5$ reaction.[16] At the same time, reaction 8, being more than one order of magnitude slower than reaction 7, $k_8 = 1.6 \times 10^{-13}$ cm^3 molecule^{-1} s^{-1},[19] does not noticeably affect the vinoxy radicals concentration during the initial period of ~3 ms even at higher O_2 concentration. This can be seen from the comparison of the CH_2CHO profiles calculated using the full reaction scheme (solid curves) and without account of the secondary reaction of CH_2CHO radicals with O_2 (dotted curves). Thus, at $t = 3$ ms the decrease of CH_2CHO concentration because of reactions 7−10 is only 7% with removed O_2 (Figure 2a) and 13% without O_2 filter (Figure 2b). As expected, switching from F to OH leads to substantial lowering of the intensity at *m*/*e* 44 compared to *m*/*e* 43 (Figure 2c). In this system, additional decay of the primary radicals takes place in reactions with NO_2:

$$CH_3CO + NO_2 \rightarrow CH_3 + CO_2 + NO \qquad (13)$$

$$CH_3C(O)OO + NO_2 \rightarrow CH_3C(O)OONO_2 \qquad (14)$$

$$CH_2CHO + NO_2 \rightarrow \text{products} \qquad (15)$$

with $k_{13} = 2.5 \times 10^{-11}$,[20] $k_{14} = 8.2 \times 10^{-1}$,[21] and $k_{15} = 1.9 \times 10^{-11}$ cm^3 molecule^{-1} s^{-1}.[21] The better fit was obtained using somewhat lower value of the latter rate coefficient, $k_{15} = 1.6 \times 10^{-11}$ cm^3 molecule^{-1} s^{-1}, closer to the lower limit of the literature value. Comparison of the CH_2CHO concentrations calculated within a full reaction scheme and without the CH_2CHO loss in reactions 9−11 gives a 3 ms difference of about 7% (dotted curve in Figure 2c). Account of reaction 15 for $[NO_2] = 2 \times 10^{12}$ molecule cm^{-3} increases this difference to 11%.

Model calculations showed that signal at *m*/*e* 75 corresponds to kinetic behavior of $CH_3C(O)O_2$ radical confirming the assignment of this line to the $CH_3C(O)O_2^-$ ion. Inspection of the calculated CH_3CO and $CH_3C(O)O_2$ profiles led to the conclusion that signal at *m*/*e* 43 is likely to consist of contributions from both CH_3CO and $CH_3C(O)O_2$. Consumption of OH radicals in reaction 1 could be monitored at *m*/*e* 17 as shown in Figure 2c′. In the present study, it was an important parameter, as the CH_2CHO yield was normalized by the reacted OH concentration. One can see that OH radical signal at *m*/*e* 17 was also observed in F + CH_3CHO +O_2 system (Figure 2b′). This effect is considered below in connection with the discussion of the mechanism of reaction 7.

Analysis of the kinetic data (Figure 3) showed that probing of CH_2CHO radicals from F and OH reactions with acetaldehyde must be done at the initial period of reaction $t < 3$ ms. For $[CH_3CHO] = 7.0 \times 10^{12}$ molecule cm^{-3}, the reaction with F is complete within 2 ms, while to complete the OH + CH_3CHO reaction in such a short time it is necessary to use acetaldehyde concentrations of the order of 10^{14} molecule cm^{-3}. However, concentrations higher than 8×10^{13} molecule cm^{-3} could not be used because of a noticeable decrease of the concentration of H_3O^+ ions in the IMR and, accordingly, a decrease of sensitivity. The CH_2CHO yield was measured using CH_3CHO concentration up to 7.7×10^{13} molecule cm^{-3} and $t = 1.7-5$ ms. As even at this highest possible CH_3CHO concentrations the reaction with OH was not completed, the degree of OH conversion, $\Delta[OH]/[OH]_0$, was determined in each case either by measurement or by calculation. Table 2 presents the results of the measurements. The data can be separated in four groups: (1) filtered O_2 and high CH_3CHO concentration; (2) background O_2 and high CH_3CHO concentration; (3) added O_2 and low CH_3CHO concentration; and (4) background O_2 and low CH_3CHO concentrations. In the third group, an added oxygen flow of 120 SCC min^{-1} corresponded to $[O_2] = 5 \times 10^{15}$ molecule cm^{-3} in the main reactor. The maximal ratio of acetaldehyde concentrations in reactions with OH and F in data groups 1 and 2 was chosen to get approximately equal reaction rates of CH_3CHO with OH and F, to have a similar impact of secondary chemistry on the concentration of CH_2CHO in both reaction systems. As the results did not differ significantly from those obtained with lower reaction rates in the OH system, we can conclude that within the used reaction times signal at *m*/*e* 44 was not strongly influenced by secondary reactions. The average value obtained for the CH_2CHO yield in reaction 1 is $\Phi(CH_2CHO) = (5.1^{+2.0}/_{-1.5})$ %. The uncertainty is obtained from the error limits of the branching ratio of reaction 2 and the uncertainty in the determination of $\Delta[OH]$ and [F]. The error connected with the possible losses of vinoxy radicals in secondary reactions essentially cancels, since at a given reaction time these losses are similar in F and OH systems. Taking into account that some measurements in two systems were done at

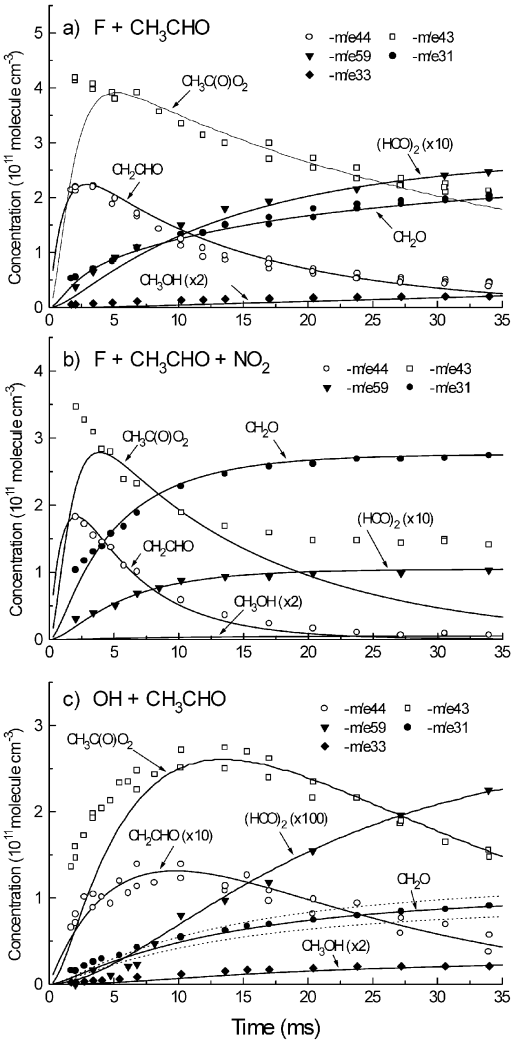

Figure 3. Time profiles of CH_2CHO (*m*/*e* 44), CH_2O (*m*/*e* 31), and $(HCO)_2$ (*m*/*e* 59) measured at $[CH_3CHO] = 7 \times 10^{12}$ molecule cm^{-3} and $[O_2] = 4 \times 10^{14}$ molecule cm^{-3}. Other initial concentrations: (a) $[F] = 0.8 \times 10^{12}$; (b) $[F] = 0.8 \times 10^{12}$, $[NO_2] = 8 \times 10^{12}$; (c) $[OH] = [NO] = 0.7 \times 10^{12}$, $[NO_2] = 1.5 \times 10^{12}$ molecule cm^{-3}. Signals at *m*/*e* 43 and 44 are also presented for convenience. Solid curves are from numerical calculation; dotted curves show the limits of fitting (see text).

TABLE 2: Measurement of the Yield of CH_2CHO Radical from the OH + CH_3CHO Reaction

												Φ(CH_2CHO) (%)	
[A][a]	$[OH]_0$	*t* ms	Δ[OH]	I_{43} cps	I_{44} cps	I_{43}/I_{44}	[A][a]	$[F]_0$	*t* ms	I_{43} cps	I_{44} cps	I_{43}/I_{44}	b	c
1. $[NO_2] = 1 \times 10^{12}$ molecule cm^{-3} (with O_2 catalytic filter)														
280	9.9	2.42	6.6	28024	1072	26.1	75	10.5	3.02	37178	10464	3.55	5.6 ± 2.2	6.9 ± 2.3
		3.02	7.3	32188	1282	25.1							6.0 ± 2.4	7.0 ± 2.4
350		2.42	7.3	32505	1173	27.7							5.5 ± 2.2	6.4 ± 2.1
640		1.81	8.4	34307	1059	32.4							4.3 ± 1.7	5.5 ± 1.8
		2.42	9.1	38084	1175	32.4							4.5 ± 1.8	5.5 ± 1.8
		3.02	9.4	39446	1176	33.5							4.3 ± 1.7	5.4 ± 1.8
2. $[NO_2] = 1.3 \times 10^{12}$ molecule cm^{-3}														
500	6.2	1.66	4.6	57156	1458	39.2	68	2.8	1.66	33577	6121	5.48	4.4 ± 1.4	7.0 ± 2.4
440	6.2	1.66	4.3	61949	1501	41.2							4.8 ± 1.6	6.7 ± 2.2
		2.21	4.9	72648	1787	40.7							5.0 ± 1.5	6.8 ± 2.3
		2.77	5.3	77975	1868	41.7							4.8 ± 1.4	6.6 ± 2.2
770	6.2	1.66	5.4	69836	1624	43.0							4.2 ± 1.0	6.4 ± 2.1
		2.77	6.0	74331	1762	42.2							4.0 ± 1.1	6.5 ± 2.2
3. $[NO_2] = 3.1 \times 10^{12}$ molecule cm^{-3} (with added O_2)														
77	8.5	1.66	1.6	20843	474	49.3	83	7.9	1.66	123319	17983	6.85	4.5 ± 1.6	7.0 ± 2.4
		2.21	2.0	21292	472	45.1							***3.1 ± 1.2***	***7.5 ± 2.5***
		2.77	2.5	27562	725	38.0			2.77	165582	9186	14.8	***3.8 ± 1.4***	***8.8 ± 2.9***
4a. $[NO_2] = 1.5 \times 10^{12}$ molecule cm^{-3}														
72	8.3	1.66	1.4	33405	2893	11.5	70	1.6	1.66	42360	12636	3.35	7.4 ± 3.3	***13.5 ± 4.5***
		2.21	1.9	36397	3356	10.8			2.21	44855	12839	3.49	6.7 ± 2.5	***14.8 ± 4.9***
		2.77	2.3	43671	3882	11.2			2.77	46225	13586	3.40	6.6 ± 2.3	***14.0 ± 4.7***
		5.6	4.1	57625	4839	11.9			5.6	45514	13656	3.33	***8.9 ± 2.3***	***13.1 ± 4.4***
4b. $[NO_2] = 2 \times 10^{12}$ molecule cm^{-3}														
65	15.4	1.66	2.4	39006	3294	11.8	65	6.8	1.66	227329	51220	4.43	5.4 ± 1.9	***16.8 ± 5.6***
		2.77	3.9	41825	3441	12.2			2.77	226864	51299	4.42	3.8 ± 1.4	***16.3 ± 5.4***
		5.6	6.2	52800	4180	12.6			4.3	211324	46402	4.55	***6.5 ± 2.4***	***16.3 ± 5.4***
											avera ge:[d]		5.1 ± 2.0	6.4 ± 1.2

[a] [A] = [CH_3CHO]; concentrations are in the units of 10^{11} molecule cm^{-3}. [b] Using OH and F calibration (see E1 in text). [c] From I_{43}/I_{44} ratio (see E3 in text). [d] Error is two standard deviations. Values in italics from experiments 3 and 4 were skipped from the evaluation as too much influenced by secondary reactions.

different reaction time and that NO_2 concentration in OH system was about 1.5×10^{12} molecule cm^{-3}, the final expression can be given as $\Phi(CH_2CHO) = (5.1^{+2.4}/_{-1.7})$ %. Some measurements, which were excluded from the estimation of the radical yield, are shown in Table 2 to demonstrate the importance of the increase of reaction time (in group 4) or concentration of NO_2 (in group 3).

Another way to evaluate the branching ratio of channel 1b is to measure the ratios of the yields of CH_3CO and CH_2CHO from reactions 1 and 2 with CH_3CO observed as a combination of CH_3CO and $CH_3C(O)OO$ signals. Calculated I_{43}/I_{44} ratios, reported in Table 2, show a difference connected with different degree of transformation of CH_3CO to peroxy form. In the experiments with added oxygen nearly full conversion takes place, giving from the reaction with OH a ratio $(I_{43}/I_{44})_{OH} \approx 49$. In the other cases, only partial conversion is observed: decrease of $[O_2]$ leads to a decrease of this ratio to about 40 at $[O_2] \cong 10^{14}$ molecule cm^{-3} and to about 30 at $[O_2] \cong 10^{13}$ molecule cm^{-3}. In the latter case, signal at *m*/*e* 43 presents mainly CH_3CO radical. The yields calculated as:

$$\Phi(CH_2CHO) = (I_{43}/I_{44})_F/\{1.86\,(I_{43}/I_{44})_{OH} + (I_{43}/I_{44})_F\} \quad \text{(E3)}$$

are given in the last column of Table 2. These values are somewhat higher than that from the calibration data, possibly indicating a systematic error of about 20% in calibration of OH and F radicals. The average yield obtained from (I_{43}/I_{44}) is $(6.4^{+3.1}/_{-2.1})$ %, where the uncertainty is due to the uncertainty of the branching ratio of reaction 2.

The branching factor for the H-atom abstraction from the methyl group of 5% corresponds to the partial rate constant $k_{1b} = 7.5 \times 10^{-13}$ cm^3 $molecule^{-1}$ s^{-1}, which appeared to be substantially higher than the theoretical transition-sate theory (TST) value obtained by Taylor et al.,[3] $k_{1b} = 1.3 \times 10^{-13}$ cm^3 $molecule^{-1}$ s^{-1}. In their work, TS geometry and frequencies were calculated at HF/6-31G(d) level and for the exponential term a value of 1.0 kcal mol^{-1} was used, equal to the empirical value derived for OH + C_2H_6 reaction. However, taking into account the existing difference in bond dissociation energies, $D_0(H-CH_2CH_3) = 99.5$ and $D_0(H-CH_2CHO) = 92.8$ kcal mol^{-1}, the energy barrier for the abstraction from the methyl group in acetaldehyde can be substantially lower. Indeed, activation energies can be correlated with the reaction enthalpies using the Marcus equation:

$$E_a = E_{int} - {}^1/_2\Delta H_0 + \Delta H_0{}^2/16E_{int}$$

where ΔH_0 is the reaction enthalpy and E_{int} is the intrinsic energy for which the available kinetic data for hydrogen atom abstraction from organic compounds by OH radical provide an estimate of about 9 kcal mol^{-1}.[22] This equation gives for reactions of OH with ethane and acetaldehyde with $\Delta H_0 = 18.6$ and 25.3 kcal mol^{-1} activation energies $E_a = 2.1$ and 0.84 kcal mol^{-1}, respectively. Following the estimations of Cohen,[23] we obtain $\Delta E_0^{\ddagger} \cong E_a - RT$, that gives for reaction 1b $\Delta E_0^{\ddagger} \cong 0.3$ kcal mol^{-1}. Thus, a barrier height lower than 1 kcal mol^{-1} for H abstraction from the methyl group in acetaldehyde, providing higher TST rate constant, does not seem unreasonable. Moreover, on the basis of ab initio calculations, D'Anna et al.[9] have concluded that abstraction of the H-atom from the methyl group can also proceed via a hydrogen-bonded complex in which O-atom of the hydroxyl radical is directed toward the methyl group, and formation of this adduct is expected to be a dominating process at low temperature. In this case, TS

TABLE 3: H_2O Signal Intensity, I_{18} (in cps), from the OH Reactions with CH_3CHO and C_6H_{12} and Obtained H_2O Yield

reactant	[reactant][a]	$[NO_2]$[a]	[OH][a]	I_{18}	$\Phi(H_2O)$ (%)
			I.		
CH_3CHO	57	3.8	0.34	944 ± 29	94.3 ± 9.8
C_6H_{12}	82			1001 ± 93	
CH_3CHO	57	3.6	0.50	1338 ± 32	98.7 ± 9.4
C_6H_{12}	82			1356 ± 123	
CH_3CHO	57	3.4	0.66	1605 ± 42	92.7 ± 7.7
C_6H_{12}	82			1732 ± 126	
CH_3CHO	57	3.2	0.87	2216 ± 39	100.7 ± 10.0
C_6H_{12}	82			2201 ± 219	
			II.		
CH_3CHO	22	1.0	1.04	115427 ± 3577	98.5 ± 5.3
C_6H_{12}	35			117136 ± 2495	
CH_3CHO[b]	32	1.4	1.51	87661 ± 1719	97.9 ± 4.2
C_6H_{12}[b]	51			89571 ± 2160	

[a] Concentrations are in the units of 10^{12} molecule cm^{-3}. [b] Experiment at $T = 248$ K.

calculations must be done using a two-step approach considering the prereactive complex as suggested by Alvarez-Idaboy et al. for channel 1a.[8]

Determination of the Branching Ratio of H_2O Forming Channels. This part of the study was performed by flowing He/SF_6 in the IMR and measuring the signal at *m*/*e* 18 which corresponded to H_2O^+ ions from water molecules formed in reaction 1. The H_2O signal from 1 was compared to that from reaction 16:

$$OH + CH_3CHO \rightarrow H_2O + \text{other products} \qquad (1)$$

$$OH + C_6H_{12} \rightarrow H_2O + C_6H_{11} \qquad (16)$$

with a unity yield of H_2O. As the rate constant of reaction 16 is 2 times less than that of reaction 1, larger concentrations of cyclohexane were used to provide more similar reaction rates. In the first experiment carried out at $T = 298$ K, the signal at *m*/*e* 18 was measured with $[CH_3CHO] = 5.7 \times 10^{13}$ molecule cm^{-3}, $[C_6H_{12}] = 8.2 \times 10^{13}$ molecule cm^{-3}, and reaction time $t = 30$ ms. Under these conditions, the characteristic reaction time was less than 2 ms, and a complete consumption of OH radicals took place in both reactions. Large excess of the molecular reactant over OH ensured that there was no contribution of H_2O formed in secondary reactions of OH radicals. Cyclohexane entered the reactor with a He flow passing through the trap with liquid C_6H_{12}, which was purified in several freeze−pump−thaw cycles. Its concentration was estimated assuming that the partial pressure of C_6H_{12} in the flow was equal to the saturated vapor pressure. The results of the measurements done for four OH concentrations in the range $(0.6-2.0) \times 10^{12}$ molecule cm^{-3} are presented in part I of Table 3. The average yield is $\Phi(H_2O) = (96.6 \pm 9.4)$ % confirming that at room temperature reaction 1 proceeds by H abstraction. The second experiment was done at $T = 298$ and 248 K, with cyclohexane introduced into the reactor from a pre-prepared mixture with He. The reactant concentrations were $[CH_3CHO] = 2.2 \times 10^{13}$ and $[C_6H_{12}] = 3.5 \times 10^{13}$ molecule cm^{-3} at 298 K and $[CH_3CHO] = 3.2 \times 10^{13}$ and $[C_6H_{12}] = 5.1 \times 10^{13}$ molecule cm^{-3} at 248 K. The measured H_2O signals are given in part II of Table 3. The obtained yields are $\Phi(H_2O) = (98.5 \pm 5.3)$ % at $T = 298$ K and $\Phi(H_2O) = (97.9 \pm 4.2)$ % at $T = 248$ K. The difference between all the measured values is within the experimental uncertainty, and the preferred value from all the data can be given as $\Phi(H_2O) = (97.7 \pm 4.7)$ % in the 298−248 K range.

This result agrees with the data of Vandenberk and Peeters[6] who obtained a (89 ± 16)% yield of H_2O in a mass spectrometric study with electron impact ionization. The present CIMS estimation narrows the probability of channels other than H-atom abstraction to less than 3% confirming that in the 298−240 K range reaction proceeds by H-atom abstraction and the increase of the rate constant with lowering the temperature can be explained by an increasing role of hydrogen-bonded prereactive complex resulting in abstraction of aldehydic H-atom as suggested by Vandenberk and Peeters[6] and Tyndall et al.[4] and confirmed theoretically by Alvarez-Idaboy et al.[8] and D'Anna et al.[9]

Kinetics of Stable Products in the OH + CH_3CHO and F + CH_3CHO Systems. Kinetics of the CH_2O, $(HCO)_2$, and CH_3OH products were studied in attempt to elucidate the unknown products formed in the reactions of CH_3CO and CH_2CHO radicals with oxygen.

Previous studies have shown that the mechanisms of both $CH_3CO + O_2$ (7) and $CH_2CHO + O_2$ (8) reactions involve competition between stabilization and decomposition of the excited acetyl- or vinoxy-O_2 adducts[17,19,24−28]. The possible pathways of reaction 7 are as follows:

$$CH_3CO + O_2 \rightarrow [CH_3C(O)OO]^* \rightarrow CH_3C(O)OO \qquad (7a)$$

$$\rightarrow OH + CH_2C(O)O \qquad (7b)$$

$$\rightarrow OH + CH_2O + CO \qquad (7c)$$

$$\rightarrow HO_2 + CH_2CO \qquad (7d)$$

Formation of OH radicals was observed by Michael et al.,[24] Tyndall et al.,[25] and Blitz et al.[17] In the present study, the OH production was confirmed by observation of signal at *m*/*e* 17 in $F + CH_3CHO$ system at higher O_2 concentrations (see Figure 2b′). The maximum measured intensity corresponded to $[OH] = 2.2 \times 10^{11}$ molecule cm^{-3}, which represented about 20% of the initial concentration of F atoms in agreement with the data of Blitz et al. that OH yield was 17% at 200 Torr and 298 K.[17]

In a smog chamber study of the oxidation of CH_3CHO,[26] Tyndall et al. found that the branching fraction of channel 7a varied from <50% at $P < 6$ Torr to about 97% at 700 Torr, but the coproducts of OH producing channels of reaction 7 were not identified. In the absence of NO_2, acetylperoxy radical from 7a gave CH_3 radical, which was predominantly converted to CH_2O. Consequently, possible production of CH_2O in channel 7c could not be distinguished from the product of CH_3 oxidation. Ketene from channel 7d was detected at very low yields less than 0.3% at 20 Torr, which allows to neglect this channel at higher pressures. The fate of the $CH_2C(O)O$ biradical is unknown. Cyclization was considered as a possible pathway,[24,25] but no characteristic bands of the cyclic structure were observed by FTIR product detection.[26] It might be expected to decompose to CH_2O and CO; in this case channel 7b represents the intermediate step of channel 7c. The authors, however, ruled out this pathway and suggested $CH_2C(O)O$ recombination with formation of a nondetectable compound. In the recent theoretical study of the $CH_3CO + O_2$ reaction using ab initio and density functional calculations of Lee et al.,[29] stabilized $CH_3C(O)OO$ adduct was the only important product at 298 K, while the formation of biradical $CH_2C(O)O$ or cyclic ketone as well as decomposition to $CH_2CO + HO_2$ appeared to be important only at high temperatures (~1000 K) because of too high calculated energy barriers.

In another FTIR product study of the OH + CH_3CHO reaction in synthetic air at atmospheric pressure,[9] CH_2O and CO were observed in the initial period of reaction as primary products with a yield of about 10%. The authors concluded that it was a result of the prompt dissociation of acetyl radical, namely,

$$OH + CH_3CHO \rightarrow CH_3 + CO + H_2O \quad (1e)$$

followed by the fast formation of formaldehyde from CH_3. However, this channel seems unlikely as CO was not observed among the products of reaction 1 in the IR chemiluminescent study.[30] The alternative explanation can be fast formation of CH_2O in reactions 7 and 8 of the primary radicals with oxygen.

In reaction 8, formaldehyde is also one of the possible products of the decomposition of the adduct of the vinoxy radical with O_2:

$$CH_2CHO + O_2 \rightarrow OOCH_2CHO^* \rightarrow OOCH_2CHO \quad (8a)$$

$$\rightarrow OH + (HCO)_2 \quad (8b)$$

$$\rightarrow OH + CH_2O + CO \quad (8c)$$

$$\rightarrow HO_2 + CH_2CO \quad (8d)$$

In the early LIF study,[27] channel 8c was considered as an alternative to 8a, and the suggested mechanism was the migration of aldehydic H-atom to the end oxygen, followed by decomposition to OH + CH_2O + CO. Zhu and Johnston[19] did observe CH_2O using cavity ring-down spectroscopy, proving the existence of reaction 8c; unfortunately, this channel was not quantified. Decomposition of the adduct can also produce glyoxal (channel 8b), which was also detected in a study of Zhu and Johnston with 15% yield at 200 Torr.[19] Time-resolved measurements of the decay of CH_2CHO and formation of $(CHO)_2$ carried out in that study gave evidence that glyoxal resulted from the isomerization of the stabilized adduct followed by decomposition.

In the present work production of CH_2O, $(HCO)_2$, and CH_3OH was measured in two chemical systems having very different CH_3CO/CH_2CHO product branching ratios. Their CIMS signals were compared with the results of numerical simulation using different branching ratios for the coproducts of the OH producing channel of reactions 7 and 8. As it was written in the Experimental Section, formaldehyde and methanol were monitored at *m*/*e* 31 and *m*/*e* 33, respectively. We did not find any report about the proton-transfer ionization of glyoxal or about either the measured or calculated value of its proton affinity. However, the PA of glyoxal is expected to be larger than PA of H_2O, and glyoxal is expected to produce signal at *m*/*e* 59 as a result of the reaction with H_3O^+.[31] Proton-transfer signal of glyoxal interferes with that of acetone, which is produced by the reaction of acetyl radicals with acetaldehyde:

$$CH_3CHO + CH_3CO \rightarrow CH_3C(O)CH_3 + HCO \quad (17)$$

However, at the used CH_3CHO concentrations, reaction 17 with $k_{17} = 2.8 \times 10^{-13}$ cm^3 molecule^{-1} s^{-1}[32] cannot compete with reaction 7. Hence, the observed signal at *m*/*e* 59 can be assigned entirely to glyoxal. Another possible product of reaction 8 is ketene, CH_2CO; however, in our detection scheme, proton-transfer signal from ketene (*m*/*e* 43) interferes with the acetyl and acetylperoxy peaks and cannot be identified. The relation between the observed intensities must be close to the relation between the rate constants of the ion-molecular reactions of the molecules with H_3O^+, which are rather similar (in cm^3 molecule^{-1} s^{-1}): 3.7×10^{-9} for CH_3CHO and 3.3×10^{-9} for CH_2O,[14] 2.1×10^{-9} for CH_3OH and 2.0×10^{-9} for CH_2CO.[13] Considering the possible reactions with water clusters of H_3O^+, the observed intensity ratios correspond within a factor of 2 to the relative concentrations in the reactor.

Figure 3 presents time profiles of CH_2O and $(HCO)_2$ products from F + CH_3CHO reaction in the absence (3a) and in the presence (3b) of NO_2 and from OH + CH_3CHO reaction 3c. All experiments were carried out without removal of oxygen from the N_2 flow. In F + CH_3CHO system (Figure 3a), the intensity of CH_2O at long reaction time was approximately the same as the maximum intensity of vinoxy radical, while the $(HCO)_2$ signal was about 10 times less. The glyoxal profile at *m*/*e* 59 was satisfactorily described by reaction 8b. The normalization coefficient for glyoxal corresponding to the branching factor $k_{8b}/k_8 = 0.15$[19] was 2.9×10^4, similar to that for CH_2CHO radical (2.3×10^4). Addition of NO_2 (Figure 3b) leads to faster decay of the radicals because of reactions:

$$CH_3CO + NO_2 \rightarrow CH_3 + CO_2 + NO \quad (13)$$

$$CH_3C(O)OO + NO_2 \rightarrow CH_3C(O)OONO_2 \quad (14)$$

$$CH_2CHO + NO_2 \rightarrow \text{products} \quad (15)$$

already considered in determination of CH_2CHO yield. At the used $[NO_2] = 8 \times 10^{12}$ molecule cm^{-3} reaction 13 still cannot compete with reaction 7, but the ultimate fate of $CH_3C(O)O_2$ radical is reaction 14. Signal intensity at *m*/*e* 43 remains at a certain stationary level, indicating that it includes a contribution from PAN. Addition of NO_2 also results in an increase of the CH_2O yield and a decrease of the $(HCO)_2$ yield. This can be explained by the fact that reaction 15 competes with reaction 8, and the likely mechanism of reaction 15 is:

$$CH_2CHO + NO_2 \rightarrow OCH_2CHO + NO \quad (15)$$

with decomposition of the formed OCH_2CHO radical to CH_2O and HCO. The presented calculation corresponds to $k_{15} = 1.6 \times 10^{-11}$ cm^3 molecule^{-1} s^{-1}, which is slightly less but within the error limits of the literature value.[21] A rapid decomposition of CH_3CO_2 to CH_3 and CO_2 and of OCH_2CHO to CH_2O and HCO was assumed in the simulation. If there were no decomposition, in the presence of NO_2 the occurrence of addition reaction:

$$OCH_2CHO + NO_2 \rightarrow OHCCH_2ONO_2 \quad (18)$$

with rate constant of about $k_{18} = 3 \times 10^{-11}$ cm^3 molecule^{-1} s^{-1} would be expected by analogy to the OCH_2CHO reaction with NO,[10] which would lead to the decrease of the yield of CH_2O with addition of NO_2.

In Figure 3c, the CH_2CHO and $(HCO)_2$ concentrations are multiplied by 10 compared to Figure 3a and 3b. It is seen that the signal of glyoxal remains unchanged with respect to the signal of vinoxy radical, whereas the intensities of CH_2O and CH_3OH noticeably increase. This increase can be explained by the relatively larger amount of the primary CH_3CO radicals produced in reaction 1 compared to reaction 2. The enhanced production of methanol in reaction with OH compared to reaction with F was simulated by incorporation of the fast recombination reaction CH_3 + OH with $k = 1.2 \times 10^{-10}$ cm^3 molecule^{-1} s^{-1}. The yield of methanol decreased with addition of O_2, in accordance with the competition between CH_3 + OH

and $CH_3 + O_2$ reactions. The measured methanol signal was scaled to calculated concentration using a normalization factor of 2.9×10^4, indicating very close sensitivities to methanol and glyoxal.

Combining data from $F + CH_3CHO$, $F + CH_3CHO + NO_2$, and $OH + CH_3CHO$ systems, the curves at *m*/*e* 31 could be fitted assuming formation of formaldehyde in reactions 7c and 8c and by varying the branching ratios of the CH_2O forming channels from $k_{7c}/k_7 = 0$ to 0.17 and from $k_{8c}/k_8 = 0$ to 0.85, and using for CH_2O a unique normalization factor of 3.2×10^4 in all three systems. In final fitting, a branching ratio of $k_{7c}/k_7 = 0.10 \div 0.15$ was obtained. Changing k_{7c}/k_7 in this range led to corresponding change of k_{8c}/k_8 from 0.30 to 0.15 when the same normalization coefficients for CH_2CHO and $(HCO)_2$ in $OH + CH_3CHO$ case were used as in fluorine system. Consequently, taking the average values, we can conclude that the CH_2O yield from reaction 7, about 12%, is slightly less than the yield of OH (17%), whereas in reaction 8 CH_2O yield, about 23%, exceeds the yield of glyoxal (15%). Sensitivity analysis showed that radical recombination reactions 9 and 10 had a little effect on the concentration of CH_2O, and only the variation of the rate constants of the reactions of CH_2CHO radical with $CH_3C(O)O_2$ (reaction 1) and NO_2 (reaction 5) could change the parameters of the fitting. The above ranges of the branching ratios correspond to variation of k_{11} in the range of $(2.5-4.0) \times 10^{-11}$ cm^3 molecule^{-1} s^{-1}, whereas k_{15} was fixed at $k_{15} = 1.6 \times 10^{-11}$ cm^3 molecule^{-1} s^{-1} as giving the best fit for the CH_2CHO kinetic curves (see also Figure 2). The dotted curves in Figure 3 show the limits of the fit owing to the variation of k_{7c}/k_7, k_{8c}/k_8, and k_{11}.

To summarize the model study, the yield of CH_2O in the reaction of CH_3CO radical with O_2 was estimated to be 10−15%. It suggests that formaldehyde is the major coproduct of OH in this reaction, for which a 17% yield was determined under similar conditions.[17] Both glyoxal and formaldehyde are produced in the reaction of O_2 with CH_2CHO radicals. Fixing for glyoxal a 15% yield as obtained in[18] a 15−30% range for the CH_2O yield was found by fitting the measured time profiles. The measurements were consistent only by assuming a rapid decomposition of OCH_2CHO radicals to CH_2O and HCO in the time scale of the experiment (>2 ms). This does not contradict the results of the study of Sehested et al.,[10] where the products of the reactions of CH_3CO and CH_2CHO with O_2 in the presence of NO were detected by transient UV absorption spectroscopy at atmospheric pressure, and where the authors deduced that no decomposition of OCH_2CHO occurred within 10^{-5} s. Comparing both results, the lifetime of the OCH_2CHO radical can be set between 10^{-5} and 10^{-3} s. Sehested et al. also found that the major product in reaction 8 was $OOCH_2CHO$ (>90%), indicating a possible decrease of the importance of channels 8b and 8c with an increase of pressure.

Conclusions

The mechanistic study of $OH + CH_3CHO$ reaction in turbulent flow reactor with mass spectrometric detection of products using proton transfer showed that hydrogen abstraction producing H_2O is the major if not the unique pathway of the reaction at $T = 298$ and 248 K. The branching fraction of the abstraction from the methyl group was about 5% at $T = 298$ K. The present study also contributes to better define the mechanism of the reaction of oxygen with CH_3CO and CH_2CHO radicals produced in channels 1a and 1b of the $OH + CH_3CHO$ reaction.

For atmospheric application, the present data confirm that acetaldehyde is a predominant source of peroxyacetylnitrate (PAN) through channel 1a of its OH-initiated oxidation. However, the branching ratio of 5% for channel 1b will lead to a slight decrease of the PAN formation potential of CH_3CHO, which is assessed so far by considering a branching fraction of unity for channel 1a. The PAN formation potential of CH_3CHO may be even lower in the upper troposphere since the branching fraction of channel 1b may increase with decreasing temperature as recently suggested.[9] This remains to be checked by extending the present measurements at low temperatures.

Acknowledgment. This work has been carried out within the EU UTOPIHAN-ACT project EVK2-CT2001-00099. We thank J. N. Crowley and J. Peeters for sending their results prior to publication.

References and Notes

(1) DeMore, W. B.; Sander, S. P.; Golden, D. M.; Hampson, R. F.; Kurylo, M. J.; Howard, C. J.; Ravishankara, A. R.; Kolb, C. E.; Molina, M. J. *Chemical kinetics and Photochemical data for use in stratospheric modeling*; Evaluation Number 12; JPL Publication: Pasadena, CA, 97−4, 1997.

(2) Sivakumaran, V.; Crowley, J. N. *Phys. Chem. Chem. Phys.* **2003**, *5*, 106.

(3) Taylor, P. H.; Rahman, M. S.; Arif, M.; Dellinger, B.; Marshall, P. *Int. Symp. Combust.* **1996**, *26*, 497.

(4) Tyndall, G. S.; Orlando, J. J.; Wallington, T. J.; Hurley, M. D.; Goto, M.; Kawasaki, M. *Phys. Chem. Chem. Phys.* **2002**, *4*, 2189.

(5) Cameron, M.; Sivakumaran, V.; Dillon, T. J.; Crowley, J. N. *Phys. Chem. Chem. Phys.* **2002**, *4*, 3628.

(6) Vandenberk, S.; Peeters, J. *J. Photochem. Photobiol., A* **2002**, *157*, 268.

(7) Berkowitz, J.; Ellison, G. B.; Gutman, D. *J. Phys. Chem.* **1994**, *98*, 2744.

(8) Alvarez-Idaboy, J. R.; Mora-Diez, N.; Boyd, R. J. Vivier-Bunge, A. *J. Am. Chem. Soc.* **2001**, *123*, 2018.

(9) D'Anna, B.; Bakken, V.; A. Beukes, J.; Nielsen, C. J.; Brudnik, K.; Jodkowski, J. T. *Phys. Chem. Chem. Phys.* **2003**, *5*, 1790.

(10) Sehested, J.; Christensen, L. K.; Nielsen, O. J.; Wallington, T. J. *Int. J. Chem. Kinet.* **1998**, *30*, 913.

(11) Atkinson, R. *Chem. Rev.* **1986**, *86*, 69.

(12) Kukui, A.; Borissenko, D.; Laverdet, G.; Le Bras, G. *J. Phys. Chem. A* **2003**, *107*, 5732.

(13) Ikezoe, Y.; Matsuoka, S.; Takebe, M.; Viggiano, A. *Gas Phase Ion−Molecule Reaction Rate Constants Through 1986*; Ion Reaction Research Group of the Mass Spectroscopy Society of Japan, Maruzen Company: Tokyo, 1987.

(14) Midey, A. J.; Arnold, S. T.; Viggiano, A. A. *J. Phys. Chem. A* **2000**, *104*, 2706.

(15) Hunter, E. P.; Lias, S. G. *J. Phys. Chem. Ref. Data* **1998**, *27*, 413.

(16) *NIST Chemical Kinetics Database*, Standard Reference Database 17, Web Version 7.0; NIST: Gaithersburg, MD, 2000.

(17) Blitz, M. A.; Heard, D. E.; Pilling, M. J. *Chem. Phys. Lett.* **2002**, *365*, 374.

(18) Hassinen, E.; Kalliorinne, K.; Koskikallio, J. *Int. J. Chem. Kinet.* **1990**, *22*, 741.

(19) Zhu, L.; Johnston, G. *J. Phys. Chem.* **1995**, *99*, 15114.

(20) Slagle, I. R.; Gutman, D. *J. Am. Chem. Soc.* **1982**, *104*, 4741.

(21) Barnhard, K. I.; Santiago, A.; He, M.; Asmar, F.; Weiner, B. R. *Chem. Phys. Lett.* **1991**, *178*, 150.

(22) Rayez, M. T.; Scollard, D. J.; Treacy, J. J.; Sidebottom, H. W.; Balestra-Garcia, C.; Teton, S.; LeBras, G. *Chem Phys. Lett.* **1994**, *223*, 452.

(23) Cohen, N. *Int. J. Chem. Kinet.* **1989**, *21*, 909.

(24) Michael, J. V.; Keil, D. G.; Klemm, R. B. *J. Chem. Phys.* **1985**, *83*, 1630.

(25) Tyndall, G. S.; Staffelbach, T. A.; Orlando, I. J.; Calvert, J. G. *Int. J. Chem. Kinet.* **1995**, *27*, 1009.

(26) Tyndall, G. S.; Orlando, J. J.; Wallington, T. J.; Hurley, M. D. *Int. J. Chem. Kinet.* **1997**, *29*, 655.

(27) Gutman, D.; Nelson, H. H. *J. Phys. Chem.* **1983**, *87*, 3902.

(28) Lorenz, K.; Rhasa, D.; Zellner, R.; Fritz, B. *Ber. Bunsen-Ges. Phys. Chem.* **1985**, *89*, 341.

(29) Lee, J.; Chen, C.-J.; Bozelli, J. W. *J. Phys. Chem. A* **2002**, *106*, 7155.

(30) Butkovskaya, N. I.; Setser, D. W. *J. Phys. Chem. A* **2000**, *104*, 9428.

(31) Williams, J.; Pöschl, U.; Crutzen, P. J.; Hansel, A.; Holzinger, R.; Warneke, C.; Lindinger, W.; Lelieveld, J. *J. Atmos. Chem.* **2001**, *38*, 133.

(32) Gill, R. J.; Johnson, W. D.; Atkinson, G. H. *Chem. Phys.* **1981**, *58*, 29.